Xu, Ying; Kujala, Pentti; Hu, Zhiqiang; Li, Fang; Chen, Gang

Numerical simulation of level ice impact on landing craft bow considering the transverse isotropy of Baltic Sea ice based on XFEM

Published in:
Marine Structures

DOI:
10.1016/j.marstruc.2020.102735

Published: 01/05/2020

Document Version
Peer-reviewed accepted author manuscript, also known as Final accepted manuscript or Post-print

Numerical simulation of level ice impact on landing craft bow considering the transverse isotropy of Baltic Sea ice based on XFEM

Ying Xu[a,b,c,*], Pentti Kujala[c], Zhiqiang Hu[d], Fang Li[c], Gang Chen[a,e]
[a] State Key Laboratory of Ocean Engineering, Shanghai Jiao Tong University, Shanghai 200240, China
[b] Collaborative Innovation Center for Advanced Ship and Deep-Sea Exploration, Shanghai Jiao Tong University, Shanghai 200240, China
[c] Marine Technology, School of Engineering, Aalto University, P.O. Box 15300, 00076-Aalto, Finland
[d] School of Engineering, Newcastle University, Newcastle upon Tyne, NE1 7RU, UK
[e] Marine Design & Research Institute of China, Shanghai 200011, China

Abstract

Ice bending is a major failure mechanism of level ice when ships and marine structures interact with level ice. This paper aims to investigate the ice bending and ice load when level ice collides on ships and marine structures using numerical simulation method, and compare the numerical results with field test. The fracture of ice is simulated with extended finite element method (XFEM), and cohesive zone concept is used to describe the crack propagation. In order to consider the characteristics of S2 columnar ice, a transversely isotropic elastic material model is used for the ice bulk elements, and a transversely isotropic Tsai-Wu failure criterion is adopted to predict the initiation of cracks. A well-controlled field test of a landing craft bow colliding with level ice in Baltic Sea is simulated to verify the numerical scheme. The ice plate's continuous deformation, crack initiation and crack propagation at different impact velocities and angles are simulated and the results are discussed. In the simulation, the bending crack emerges at the midline of the top surface of ice plate, then propagates towards free boundary, and finally a circumferential crack forms. It is found that with the impact velocity increases, the bending load increases and the fracture size (perpendicular distance from the crack to the contact edge) decreases. And as the angle between the landing craft bow and vertical direction increases, the bending load and the fracture size decrease. The simulated results corresponds well with the field test. The competition between the circumferential crack and radial crack is also found in the simulation and will be discussed in this paper. The results show that this method well simulates the bending of level ice and predict the ice load, and provides a good approach for investigating the mechanism of different forms of level ice fracture.
Key words: Level ice; Bending; Ice load; Extended finite element method; Transversely isotropic.

1. Introduction

Maritime activities in the polar regions have considerable economic prospects. Whether it is ship navigation or resource exploitation in the cold regions, it is inevitable to encounter the interaction of ships or marine structures with level ice. Predicting the ice load caused by level ice is necessary, and numerical simulation is a powerful method to achieve this purpose. While one of the characteristics of ice is that its tensile strength is much smaller than the compressive strength, and sloping shape is a common feature of ships and marine structures. These factors make level ice very easy to fail in bending. Therefore, bending fracture is a main failure mechanism of level ice and an important mechanism of limiting the ice load. However, simulating ice cracks is always a challenging task, and reliable comparison with experiments is far more from sufficiency. This paper aims to use numerical method to investigate the bending failure of level ice, and validate the numerical results with a field test. Meanwhile, the relation between bending crack and radial crack, and their initiation and propagation processes will be discussed. Extended finite element method (XFEM) combining with a transversely isotropic ice model is used to simulate cracks and obtain ice load.

Typical scenarios where bending failure occurs include a ship sailing in level ice, and level ice pushing towards an inclined component of marine structures (anti-ice cone). The understanding of an individual bending event or a single bending crack of level ice is of great benefit to the investigation of these problems. However, current research on this issue is still limited. Some studies are based on empirical formulas or analytical methods for the plate and beam.

Lindqvist [1] proposed a straightforward method to calculate the ice resistance on ships, in which a simple formula that it is related to the ship hull, ice thickness, ice characteristic length was established to calculate bending load. However, the method based on empirical formula can't reflect the bending mechanism of level ice. Kerr [2-5] summarized several analytical solutions to determine the bearing capacity of ice plates. It was assumed that the ice plate was elastic and viscoelastic, then the analytical

* Corresponding author. State Key Laboratory of Ocean Engineering, Shanghai Jiao Tong University, Shanghai 200240, China.
E-mail address: xuyingxyy@163.com (Y. Xu).

solutions of ice plate under different loading and boundary conditions were discussed. One of the main conclusions was that the bending load was related to the angle of ice wedge, ice thickness and bending strength. This conclusion was used in many numerical simulations to determine the ice load induced by bending failure. One of them was that Biao et al. [6-7] applied this bending equation to investigate the ship performance in level ice. Zhou et al. [8] also adopted this equation to obtain the ice load of the ice breaking and accumulation. In addition to this, Lubbad and Loset [9] proposed a closed analytical solution for the maximum bending stress of a semi-infinite ice sheet when the load is distributed uniformly over a half circular area, to simulate real-time ship-ice interaction. While Erceg [10] proposed a quasi-static numerical method to model the initiation of circumferential cracks of level ice. It was assumed that the level ice can be discretized as radially oriented ice beams from the contact zone, and the ice beam is modeled as semi-infinite beams resting on elastic foundation. Wang and Poh [11] adopted Euler-Bernoulli beam theory for level ice and potential fluid theory to simulate ice-wide sloping structure interaction and investigate the velocity effect on ice bending.

The above solutions are mainly based on empirical equations or static analysis. While level ice bending caused by ships occurs mostly at high speeds, and the actual material properties of level ice is too complicated to be fully considered in analytical method. Ehlers and Kujala [12] used a plastic model and element deletion technique in LS-DYNA to simulate the bending failure of ice beam. The material model that differed the tensile and compressive constitutive relationships was used to capture the different characteristics of tensile and compressive failure of ice. While the bending of ice beam was quite different from the bending of ice plate, Sazidy [13] applied similar tensile-compressive plastic model and element deletion method to simulate bending failure of level ice wedges, and the strain rate effect on compressive behavior was considered. In that investigation, it was assumed that the ice plate bending was divided into two stages: radial cracking that cuts ice plate into ice wedges, then circumferential cracking to make the ice plate bend. However, it is well known that the form of the structure has significant influence on the ice failure mode. The two-step failure assumption may be suitable for the interaction of ice plate with narrow columnar structures, such as the anti-ice cones, in which condition the level ice contacts with the curved structure in a small and concentrated area compared to the size of ice plate. While for the interaction with ships and structures that usually have relatively flat hull, the contact way is different and the interaction force is distributed along the ice plate edge. In this condition, the relation between circumferential crack and radial crack needs to be further investigated. For example, the ice near the ship hull when the ship sails in level ice often undergoes continuous bending, so circumferential crack is a main mechanism of ice failure. However, it has rarely been discussed whether radial crack emerges and what is its relation with bending crack.

In this paper, the field test that a landing craft bow collides with shaped level ice will be simulated. This field test was conducted by Technical Research Center of Finland (VTT) and Rauma-Pepola Oy in Baltic Sea [14]. In this test, a tug arranged with an artificial landing craft bow moved in horizontal direction until slammed into the level ice. Finite element analysis was conducted in [14] to predict the location of initial crack and the corresponding ice load, but the crack was not simulated. This field test is similar to the scenario of the ship navigating in level ice area, and can serve as a reference for level ice interacting with wide structure as well.

Extended finite element method (XFEM) is used to simulate cracks' initiation and propagation. XFEM originates from finite element method, but uses enrichment functions to introduce additional degrees of freedom of displacement, so the element can split. Because the crack can pass through the interior of an element in XFEM, the propagation of a crack can be well presented. XFEM retains the advantages of finite element method in description of continuous deformation, and can solve the problem of discontinuity caused by fracture. XFEM has been widely applied to the investigation of hydraulic fracturing of rocks in shale gas mining. For ice, Lu et al. [15] used XFEM to simulate the splitting crack of floe ice and obtain results consistent with field measurements. He also compared different numerical methods in simulating ice wedge bending, including element deletion, cohesive element method (CEM), discrete element method (DEM) and extended finite element method (XFEM) [16]. Compared to the other three methods, XFEM is characterized by the merits that the crack's initiation and propagation can be well presented and no re-mesh is needed, thus has the potential to simulate the crack propagation path more realistically.

The innovation of this paper is that a numerical method is proposed to simulate the bending crack of level ice and to predict the ice load, and a well-performed field test is used to validate the scheme. The comparison between simulation and field test of ice bending has been rarely done in the previous investigation, and this research will make up for this deficiency. Meanwhile, the formation mechanism of bending crack and radial crack, and the features of their initiation and propagation processes are discussed, some valuable conclusions are obtained.

When using XFEM to simulate cracks, an appropriate crack initial criterion is required to determine the emergence of the crack, and an ice material model is needed to describe the behavior of ice bulk elements. In order to simulate the ice behavior properly, the ice material model and the initial fracture criterion take into account the transversely isotropic characteristics of the ice in Baltic Sea. Cohesive surface concept with traction-separation curves is used to simulate the crack propagation.

In the following context, Section 2 sequentially states the numerical method and the constitutive relation used to simulate the crack, the material model for ice bulk elements and crack initial criterion, and the treatment of the ice crushing in contact area in bending simulation. Section 3 introduces the field test 'ice impact on landing craft bow' and the finite element model. Section 4 discusses the simulation results and compares them with the test results.

2. Method

This section will firstly introduce the extended finite element method (XFEM) and the constitutive relation of describing the crack. Then Section 2.2 and 2.3 will introduce the ice material model and initial crack criterion taking the transversely isotropic characteristics of S2 ice into account. The final part will clarify the treatment of ice crushing in contact area.

2.1 Simulation of cracks: extended finite element method (XFEM) and cohesive surface concept

Extended finite element method uses enrichment functions (equation 1) to introduce additional freedom to enable the displacement discontinuities, and uses level set method to describe the crack geometry. In this way, a crack can pass through the interior of the element.

$$\boldsymbol{u} = \sum_{I=1}^{N} N_I(x)[\boldsymbol{u}_I + H(x)\boldsymbol{a}_I + \sum_{\alpha=1}^{4} F_\alpha(x)\boldsymbol{b}_I^\alpha] \tag{1}$$

where $\boldsymbol{u}$ is the displacement vector, $N_I(x)$ and $\boldsymbol{u}_I$ are usual nodal shape function and nodal displacement vector; $\boldsymbol{a}_I$ and $\boldsymbol{b}_I^\alpha$ are the introduced freedom vectors; $H(x)$ and $F_\alpha(x)$ are discontinuous jump function across the crack surfaces and elastic asymptotic crack-tip function [17].

The principles of XFEM can refer to [18], and is not introduced in detail here. However, it is necessary to clarify the constitutive model of the crack.

The crack simulation includes crack initiation and propagation, and the latter phase requires criteria to determine whether the crack extends and in which direction it extends. Stress based Tsai-Wu criterion as described in Section 2.3 is used as the crack initial criterion. While once the crack emerges, cohesive surface concept is adopted to describe the crack propagation. Cohesive surface concept uses traction-separation curve to describe the relation of the two crack surfaces, so it also can be named as the constitutive model of the cracks. Traction (T) refers to the traction force between the two crack surfaces, and separation distance (δ) refers to the opening distance of the pair of crack surfaces. Crack propagates in the direction that is perpendicular to the maximum principle stress in this paper.

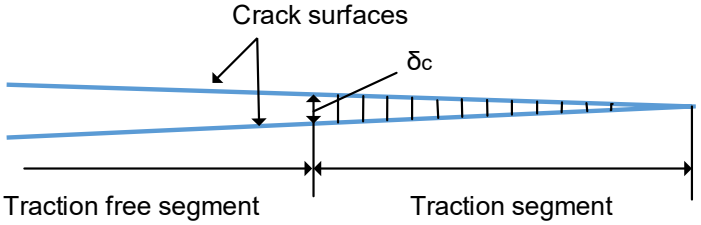

Figure 1. Cohesive surface concept of the crack surfaces. (reproduced from [28])

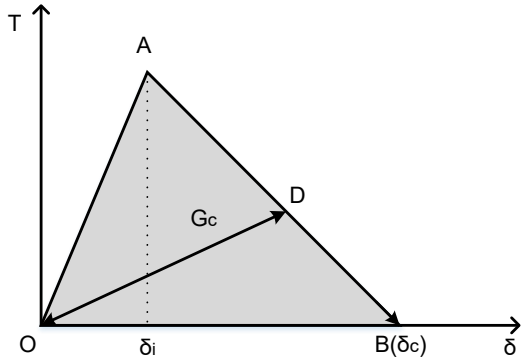

Figure 2. Traction-separation curve for the crack. (reproduced from [17])

Cohesive surface concept provides an effective and flexible way to describe the behavior of the crack, and fits well with XFEM. A schematic of the concept is shown in Figure 1. The physical meaning of cohesive surface concept can refer to the interpretation of 'fictitious crack model', which has been applied

to describe the crack of sea ice in the investigation of [24-28]. More detailed explanations and schematics of this theory can refer to [28]. The main thoughts and assumptions are as follow: The ice in front of the tip of the real crack is not intact but with micro-cracks. And in order to consider the effect of the micro-cracks on crack propagation, it is assumed that the length of the real crack is extended for a segment, then it is called as 'fictitious crack'. For the real crack, there is no traction between the fracture surfaces that has been separated. While for the fictitious crack, it is assumed that the traction still exists between the crack surfaces of the segment near the fictitious crack tip, to represent the resistance and the influence of the inelastic deformation ahead of the crack [24]. The traction-separation displacement curve is used to describe the traction force, as shown in Figure 2. The traction will become 0 when the crack surfaces opens to the critical distance. An important parameter of this relation is the fracture energy G_c, which can be represented by the area under the curve as shown in Figure 2. Fracture energy indicates how much energy is released for per unit crack area in crack propagation. It's unit is N/m. Dempsey [27-28] combined the fictitious crack model with viscoelastic bulk model to describe the tensile fracture of first year sea ice, and found it is consistent with the fracture of ice.

Cohesive surface concept is also used in other numerical techniques to simulate ice breaking and crushing [19-23], such as cohesive elements method. Cohesive elements can be inserted between ice bulk elements, and is also described with traction-separation curve. The bulk elements are separated after the cohesive elements fail, then the gap between the remaining bulk elements represents the crack. Therefore, fine meshing is required to simulate the crack path accurately. Combining with XFEM, cohesive surface concept can be used for the simulation of ice fracture. Unlike the cohesive element method, the crack can pass through the interior of the bulk element in XFEM by enrichment functions, and cohesive surface concept is applied for the description of the pair of crack surfaces.

In this paper, the traction-separation law assumes initially elastic behavior followed by damage initiation and damage evolution, as shown in Figure 2. Damage represents the degradation of the traction between the two crack surfaces. Damage initiation refers to the point of the curve at which the traction begins to degrade. And the damage evolution law describes the rate at which the cohesive stiffness degrades once the damage initiation criterion is reached.

A traction-separation curve describes the constitutive relation of the crack surfaces as follow: At the beginning, traction force between the crack surfaces rises according to linear elastic relationship. At this phase, the traction is related to separation through a cohesive stiffness matrix $\boldsymbol{K}$, which can be determined by the material property of the ice bulk elements.

$$\begin{Bmatrix} T_n \\ T_s \\ T_t \end{Bmatrix} = \begin{bmatrix} K_n & 0 & 0 \\ 0 & K_s & 0 \\ 0 & 0 & K_t \end{bmatrix} \begin{Bmatrix} \delta_n \\ \delta_s \\ \delta_t \end{Bmatrix} \tag{2}$$

where T_n, T_s and T_t are normal traction and the two shear tractions. δ_n, δ_s and δ_t are normal separation and two shear separations. K_n, K_s, and K_t are the corresponding cohesive stiffnesses.

Once reach the damage initial criterion (point A), the cohesive stiffness will degrade according to a specific damage evolution law, which is linear in this paper as shown in Figure 2. Then the traction can be presented as,

$$\bar{\boldsymbol{T}} = (1 - D)\boldsymbol{T} \tag{3}$$

where $\bar{\boldsymbol{T}}$ is the traction vector in damage phase, $\boldsymbol{T}$ is the traction vector if there is no damage and calculated according to the linear elastic relation. A scalar variable D represents the damage, and its value will rise from 0 to 1 after the damage initiation, corresponding to the traction decreasing from the highest value to 0.

After the critical separation δ_C is reached, the interaction between the crack surfaces disappears completely and traction decreases to 0. If the two surfaces between which the traction has completely vanished re-contact with each other, the surfaces will not re-connect, which means the traction will not reappear, but only friction. Before that, if the unloading occurs during the traction decrease phase, causing the surfaces to stop separating, the traction will return to zero along the shortest linear path (line DO). If the crack re-separates in the subsequent process, traction force will reload along the route (line OD) onto line AB. Because the cohesive stiffness in elastic phase can be calculated using the ice bulk material model, the damage initiation point and the traction-separation curve in damage evolution phase can be calculated automatically by specifying the value of the fracture energy and the damage evolution law.

2.2 Transversely isotropic elastic constitutive model

In order to capture the behavior of ice bending, it is necessary to adopt an appropriate ice material model. The ice material model used in the numerical analysis should be consistent with the basic mechanical properties of the sea ice. The field test simulated in this study is located in Baltic Sea, where the ice is S2 columnar ice with low salinity. The characteristics of S2 columnar ice is that the ice grains

are columnar shaped along vertical direction. This microstructure makes its mechanical properties isotropic in horizontal plane, and anisotropic in vertical planes. There may be micro-cracks, as well as brine pockets and brine channels that usually form vertically in sea ice, but these factors do not change the directionality of the ice as a whole. It is difficult and inefficient to include all these features in the numerical simulation. Therefore, it is assumed in this paper that the pores and defects inside the ice are evenly distributed, and the influence is merged in the mechanical parameters such as elastic constants. Considering the above factors, a transversely isotropic ice material model is appropriate.

Another factor to be considered is whether ice can be treated as an elastic material. At different loading velocities, ice constitutive relation could be different. From the perspective of macroscopic phenomenology, the behavior of ice is visco-elastic under low strain rates and elastic-brittle under high strain rates [29]. The moving speed of the landing craft bow to be simulated in this paper is between 1m/s and 5m/s. In these conditions, the deformation of ice is quite fast. Level ice keeps intact and produces continuum deformation, transmitting stresses to further part until fracture emerges, thus can be simplified as elastic, except for ice in contact area and along the surfaces of cracks. The deformation in the two areas is not elastic. The ice in contact area is crushed and will be discussed in Section 2.4, while traction-separation relation has been introduced in Section 2.1 to describe the crack behavior.

Combining the directionality and elastic property of S2 columnar ice, a transversely isotropic linear elastic model can be used to describe the constitutive relation of ice bulk elements. According to the symmetry of stiffness matrix and ice microstructure, there are only five independent elastic constants to link the stress matrix and strain matrix.

$$\sigma_i = c_{ij}\varepsilon_j \quad i,j = 1,2,...6. \tag{4}$$

$$c_{ij} = \begin{bmatrix} c_{11} & c_{12} & c_{13} & & & \\ c_{12} & c_{11} & c_{13} & & 0 & \\ c_{13} & c_{13} & c_{33} & & & \\ & & & c_{44} & & 0 \\ & 0 & & & c_{44} & \\ & & & 0 & & (c_{11}-c_{12})/2 \end{bmatrix} \tag{5}$$

where σ_i and ε_j represent the components of stress and strain. c_{ij} refers to the elastic constants, representing the stress in direction i induced by the strain along direction j.

The elastic constants can also be expressed with Yong's modulus E_i, shear modulus G_{ij} and Poisson's ratio ν_{ij}, which represents the strain in direction j induced by unit strain in direction i when loading in direction i. The values of these parameters used in this paper come from the experiment on Baltic Sea ice and are listed in Table 1. The nominal temperature is -6°C. In the rectangular coordinate system for the ice model, it's defined that the direction 3 is parallel to the direction of ice crystals growing (vertical), and direction 1 and 2 refer to the axes in the basal plane where ice properties are isotropic (horizontal).

Table 1. Elastic constants of S2 columnar ice of Baltic Sea [14].

Elastic constants	E_1	E_3	ν_{12}	ν_{13}	G_{13}
unit	Gpa	Gpa	-	-	Gpa
value	7.28	10.16	0.59	0.34	2.48

Note: Temperature is -6°C.

2.3 Transversely isotropic Tsai-Wu failure criterion

Tsai-Wu criterion is thought an effective macroscopic mechanical failure criterion to describe the ice failure, and is adopted as the criterion of crack initiation here. It can describe different failure modes of ice in three dimensional stress space, including tension, compression and shear failure. Compared to other common failure criteria that are usually for steel or some geologic materials like rocks and soils, it can reflect the unique characteristics of ice, including the anisotropy and the sensitivity of ice strength to hydrostatic pressure. There have been many ice strength experiments that the results were found to fit well with Tsai-Wu criterion [14, 30-31].

The Tsai-Wu failure criterion adopted in this paper is based on stress state. The general form of this criterion can be represented as follow, and when $f \geq 1$ the failure criterion is met and crack initiates,

$$\begin{aligned} f = {} & F_{11}(\sigma_1+\sigma_2) + F_{33}\sigma_3 + G_{1111}(\sigma_1^2+\sigma_2^2) + G_{3333}\sigma_3^2 + 2G_{1122}\sigma_1\sigma_2 + 2G_{1133}(\sigma_1+\sigma_2)\sigma_3 \\ & + 4G_{1313}(\sigma_4^2+\sigma_5^2) + 4G_{1212}\sigma_6^2 \end{aligned} \tag{6}$$

where F_{ij} and G_{ijpq} are mechanical parameters in failure criterion.

Due to the transversely isotropy of Baltic Sea ice, the determination of the mechanical parameters of the failure criterion requires several basic ice strength tests, including uniaxial and tri-axial compressive tests that are parallel, perpendicular and inclined to the ice axis respectively, as well as tensile tests. The necessary ice strength tests have been suggested in [14], including various kinds of compressive tests and tensile or bending tests. The measured independent ice strength values can be transformed to the mechanical parameters F_{ij} and G_{ijpq} in the failure criterion. The suggested values in [14] are illustrated in Table 2.

Many first-year sea level ice encountered by ships and marine structures is S2 columnar ice. Although most sea ice generally has higher salt content than Baltic Sea ice, transversely isotropic is the basic attribute of S2 ice. Therefore, the material model and failure criterion adopted in this study also have reference value for the analysis of first year sea ice in other areas.

Table. 2. Mechanical parameters in Tsai-Wu failure criterion [14].

Tsai-Wu parameters	unit	value
F_{11}	MPa^{-1}	1.550
F_{33}	MPa^{-1}	0.806
G_{1111}	MPa^{-1}	0.491
G_{3333}	MPa^{-2}	0.194
G_{1122}	MPa^{-2}	-0.395
G_{1133}	MPa^{-2}	0.062
G_{1313}	MPa^{-2}	0.345
G_{1212}	MPa^{-2}	0.443

Note: The temperature is -6°C .

2.4 Simplification of ice crushing in contact area

Before the occurrence of ice plate bending, the ice edge is crushed and the crushing force is rising. Simulating crushing and fracturing of ice simultaneously is difficult. Because ice crushing is accompanied by spalling and generation of ice debris, and it is challenging to simulate this phenomenon using finite element method. At present, there are literatures on using plastic material model and element deletion to obtain pressure-area relation of ice collision [32-34]. For the simulation of bending of ice plate, the ice crushing phenomenon can be simplified while retaining the main features of the crushing force rising process.

One of the feature is that the contact between inclined ship and level ice edge is line contact, especially for the case simulated in this paper. The contact area is a narrow and long area, which is different from that of the collision between a ship and icebergs as well as many indentation tests [35-37] using spherical indenters, where the contact area is generally composed by high-pressure zones with similar length and width.

Besides, the forward ship will push water onto the level ice, and water may also influence the crushing force on ice edge. During 1981 and 1982, crushing experiments and related data analysis have been done to investigate the 'line contact problem' [14]. The ice was taken from the sea around the pilot station of Ajos in Baltic Sea, same as the ice used in the experiments determining the material constants above. The ice block was fixed, and the inclined stiff striker was pressed into the ice edge. The experiments without water (dry experiment) and with water spraying on the contact area (wet experiment) were conducted to study the influence of water on contact force. The analysis established the average 'pressure-crushing depth' relation, in which the pressure is exponential with the crushing depth ($p = m\xi^{-n}$, ξ is crushing depth, n and m are constants).

The crushing experiment found that the influence of water on contact force could be significant. The pressure in contact zone when water is fully considered is higher than the dry pressure, and the final average pressure-crushing depth curve is more flat. After multiplying the pressure and area, the resultant force-crushing depth relation is close to linear within the limited depth. Based on the above observation, considering that the ice plate simulated in this paper is thin (0.36m), and the crushing depth before bending is shallow, the contact force is simplified to a linear monotonically increasing force with crushing depth, acting along the upper edge of the ice plate in contact area.

The longitudinal section of the contact area of the bending level ice with is shown in Figure 3. The force-crushing depth relation used here can be presented as,

$$F = B\xi \tag{7}$$

where ξ is the crushing depth, which is the vertical distance between the original ice upper edge and the ship plate; B is the crushing stiffness (unit: MN/m). And in the subsequent simulation of the impact of

landing craft bow on ice plate, the direction of the contact crushing force is perpendicular to the flat landing craft bow.

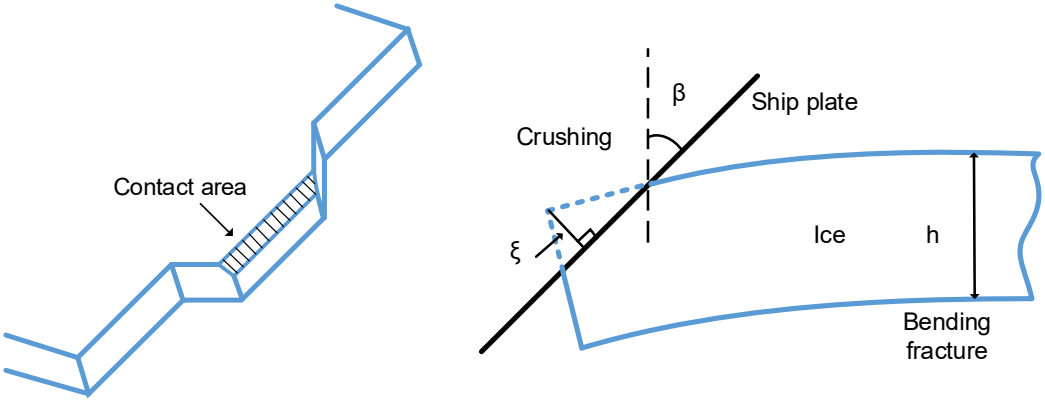

Figure 3. Schematic diagram of the contact area (left) and longitudinal section of bending level ice (right). h is the ice thickness, β is the angel between ship plate and vertical direction, ξ is the crushing depth.

3. Field test and numerical modeling

3.1 Field test of landing craft bow impact on level ice

A field test of the landing craft bow impact on level ice in the coast of Baltic Sea was performed by Technical Research Center of Finland (VTT) and Rauma-Pepola Oy, to investigate the influence of speed and angle of ship on level ice [14]. In the test, an artificial landing craft bow was installed at the front of the tug Rauma I. The angle of the artificial bow can be adjusted and controlled, and the force can be measured through the supporting system. The tug moved towards the level ice in the horizontal direction at certain speeds. Figure 4 shows the sketch of the landing craft bow impact test.

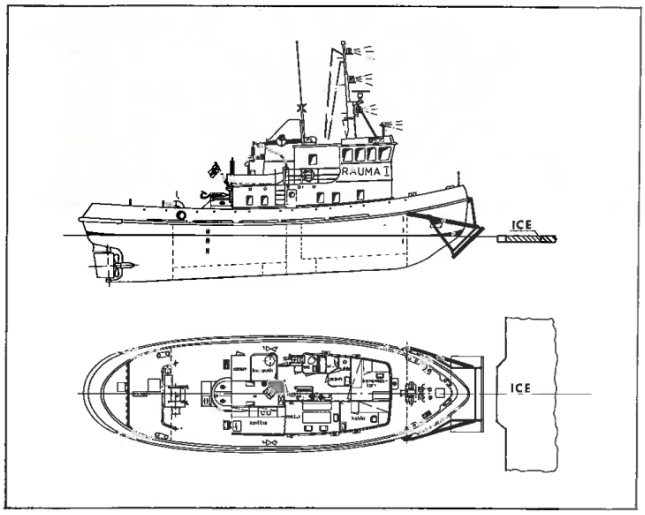

Figure 4. Sketch of the landing craft bow installed at the front of Rauma I [14].

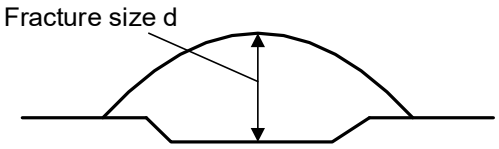

Figure 5. The distance between contact edge and bending crack recorded in the field test.

The size of the landing craft bow was 5m long and 2.5m wide. In all the test groups, the level ice were shaped to the same geometry, as shown in Figure 4 and 6. The length of the ice wedge edge was 3.5m, the wedge depth was 0.5m and the open angle was 45^{o}. The thickness of the natural level ice varied in a certain range, it was between 0.3m and 0.42m. The temperature on the top surface was around -2°C to -6.6°C. A total of 29 groups of tests were conducted, of which 9 groups were with the angle β of 30^{o} between the landing craft bow and level ice, and 20 groups were with 50^{o}. The speed of the tug was between 0 to 3.5m/s. The test recorded the ice load at different angle and velocity, as well as the distance d between the contact edge and the bending crack, as shown in Figure 5.

3.2 Extended finite element model and parameters

The numerical simulation is conducted with ABAQUS implicit dynamic analysis. Enrichment properties are applied in the area where cracks may emerge.

3.2.1 Model size and boundary conditions

The finite element model is symmetrical. The size of the modeled ice plate is shown in Figure 6. In the field tests, the size of the whole level ice is infinite compared to the size of the ship and bending area, and the boundary of level ice can be treated as fixed in the far field. The length and width of the ice plate modeled here is as large as 180m? 0m , and the three boundaries (AB, BC, CD) are fixed, the rest edges are free. The water buoyancy is simulated as springs at the bottom of the ice plate, while hydrodynamic effect is not considered in this simulation. The thickness of ice plate is taken as the average value as 0.36m. The landing craft bow is simplified as a rigid plate with size of 5m? .5m , moving at a constant velocity in horizontal direction towards the ice plate. The finite element model of the ice plate is shown in Figure 6 (right).

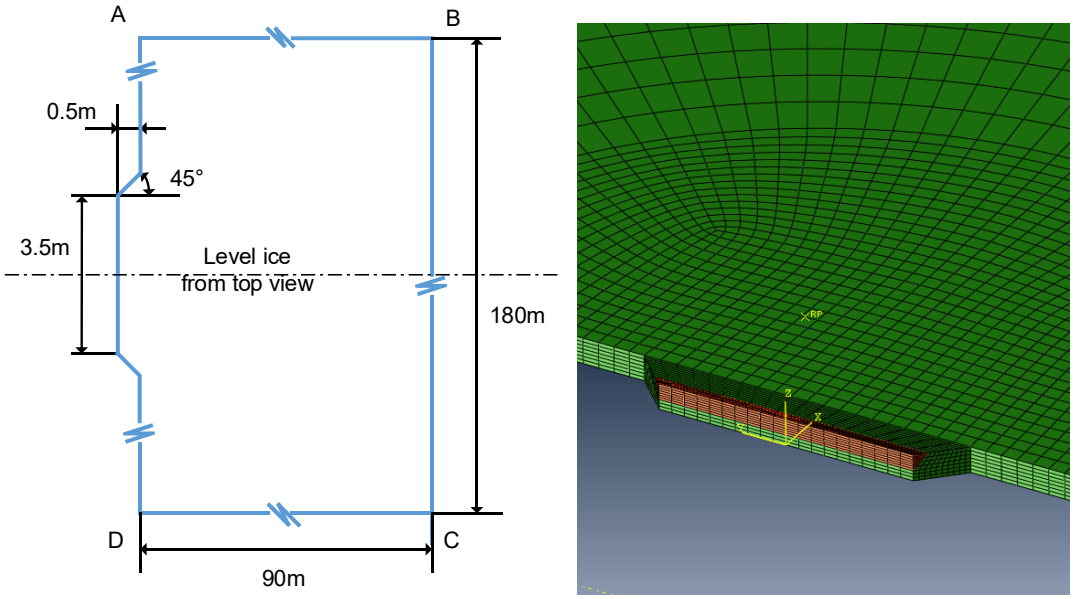

Figure 6. Geometry and size of the ice plate model (left), and finite element model of the ice plate (right). Enrichment properties are applied in the green area. Over-closure contact with the red area.

3.2.2 Crack setting and material parameters

The water density is 1025kg/m^3, and the ice density is 900kg/m^3. The ice material parameters have been given in Table 1.

No initial crack is preset. The initiation of the crack depends on Tsai-Wu criterion as clarified in Section 2.3 and the parameters are given in Table 2. Fracture energy is 5N/m [38-39]. According to the test, the area where cracks may emerge is around the contact edge, including the corner of the wedge portion. Therefore, enrichments properties are defined within a circle area with center at the middle of contact edge and radius of 4m, except for the very thin area along the contact edge between landing craft bow and level ice, shown in red in Figure 6. The failure mode along this contact area is crushing, rather than the fracture that limits the ice load. So it is assumed the crack will not emerge within the contact area, and over-closure contact is set here as stated in Section 2.4. The friction coefficient is 0.1. Due to the flat shape of the landing craft bow, the relative tangential movement in horizontal direction between the artificial bow and level ice can be avoided [14]. This design is convenient for the observation and measurement, and conductive to numerical simulations.

3.2.3 Mesh size sensitivity analysis

First-order reduced-integration solid element is used for the simulation. At present, there are still some restrictions on the application of XFEM in ABAQUS, that the enrichment properties are only available for solid continuum elements. In order to capture the bending of ice plate more accurately, the ice plate should be divided into as many levels as possible in thickness direction. 7 layers of elements are used in this paper, same as Lu et al. [15]. Considering computation efficiency and accuracy comprehensively, different regions are meshed with different grid sizes. Fine mesh is used within a circle area with center at the middle of contact edge and radius of 4m. It is shown in red in Figure 6. While coarse mesh is used for the portion far away from the circle area, and compromised mesh size for the transition area.

XFEM is based on finite element method, and can't completely overcome mesh sensitivity. In order to determine acceptable mesh size, impact at β=30° and v=3m/s is simulated using different mesh sizes.

Comparison of the fracture size and contact force is shown in Table 3. The analysis shows that the fracture size d is stable for the mesh sizes adopted here. The force of cracking through the top surface of the ice plate is lower as the mesh is finer. But for the mesh size of 0.4m? .45m and 0.2m? .2m , the simulated results are quite similar. It seems that as long as the mesh is not too rough to capture the stress field, the crack path can be simulated stably. In the following analysis, in order to analyze the competition between circumferential crack and radial crack, the mesh size of 0.2×0.2 is used.

Table 3. Simulation results of the case v=3m/s, β=30° at different mesh size.

mesh size (m)	Contact force (MN)		fracture distance d (m)
	crack initiation	crack propagation through the top surface	
1×0.6	0.450	0.728	2.20
0.67×0.45	0.436	0.557	2.17
0.4×0.45	0.415	0.524	2.3
0.2×0.2	0.412	0.519	2.2

4. Analysis and discussion

4.1 Results

The impact at different angle β (30° and 50°) and velocity v (1.2m/s, 2m/s and 3m/s) are simulated. The discussion of the results focuses on several aspects: the deformation and stress field before crack emerges, crack initiation, crack propagation path, and the corresponding ice load.

4.1.1 General bending process

The simulated deformation of the ice plate can be divided into three phases: continuous deformation, crack initiation and crack propagation. Take the case of β=50° and v=2m/s as an example, the vertical displacement at 7ms when the crack initiates is distributed as shown in Figure 7. Since the impact starts, the continuous deformation process lasts for 7ms until the initial crack emerges at 1.8m from the ice edge along the midline on the top surface of the ice plate. Along the centerline, the vertical displacement is negative at the contact point, which means the landing craft bow pushes down the ice plate here. At around 3m in the midline, the level ice is squeezed upward, and gets to 0 in far direction, showing the characteristics of buckling. After the crack initiates, it begins to propagate towards the free boundary, and finally an arc-shaped crack forms as displayed in Figure 11. This shape fits well with the field test shown in Figure 5. The simulated contact force-time history of the case of β=50° and v=2m/s can be found in Figure 8. The contact force for crack initiation is also shown as the middle point in the lines. It takes 5.2ms from the crack initiation to crack penetration through the top surface. The total time from contact to crack propagation is 12.2ms at this case, indicating that the cracking process is very fast.

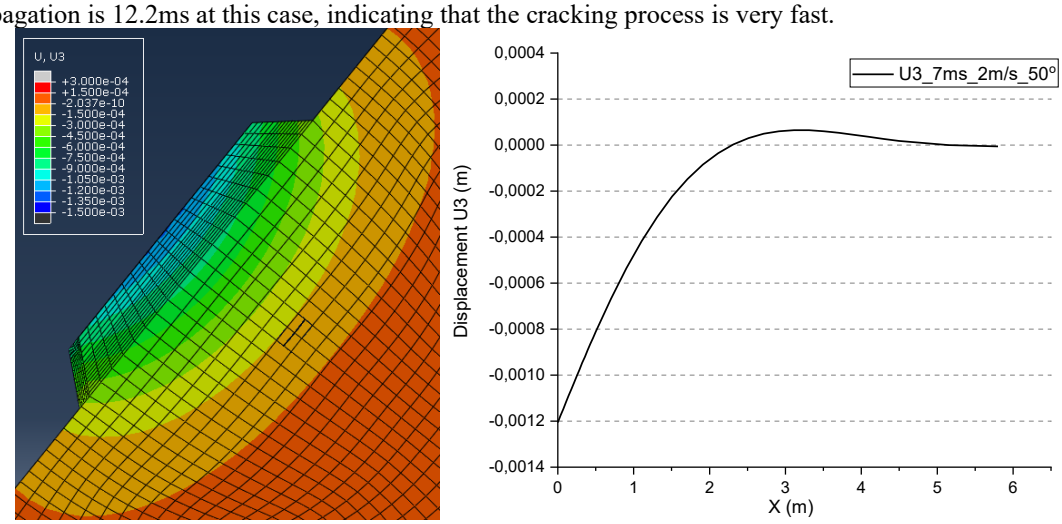

Figure 7. The ice plate displacement U3 in vertical direction at 7ms after impact (left), and its distribution along the center line (right). (β=50° , v=2m/s)

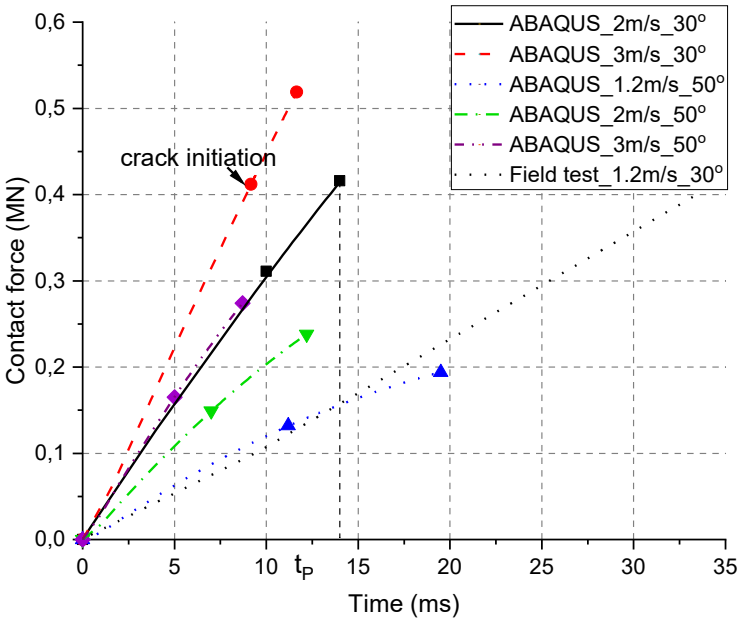

Figure 8. Simulated contact force-time curve of the ice plate under different angle β and velocity v. 0 represents the beginning of the contact, the maximum values represent the simulated ice load when the crack penetrating through the top surface of the ice plate. The contact force for crack initiation is also shown as the dot in the middle of the curve.

4.1.2 Ice load and fracture size at different impact angle and velocity

Figure 8 illustrates the simulated time history of contact force rising process of impacts at different speed and angle. t_p represents the total time from beginning of contact between ice plate and landing craft bow to the crack penetrating through the top surface of the ice plate. In all the simulated cases shown in Figure 8, the circumferential fracture is simulated successfully. And the faster the impact speed, the higher the ice load and the shorter the time it takes. For example, it takes 14ms for a circumferential curve to form and the maximum force reaches 0.42MN at the speed of 2m/s and β=30° . While at the speed of 3m/s and the same angle, the time length is 11.5ms and the maximum ice load is 0.52MN. The effect of speed on ice load is important for the operation and safety of ships in ice covered areas [40-41]. The speed effect in the simulation here only comes from the dynamic response of the ice plate, since the hydrodynamics is not considered.

The only history curve of contact force in the field test we can obtain from the report of Varsta [14] is for the case of β=30° and v=1.2m/s . It takes around 34ms for the contact force to rise to the maximum value. While in the simulation of this case, the simulated crack doesn't emerge at the top surface but at the bottom of the ice plate, which means a radial crack is prone to form rather than a circumferential crack.. This phenomenon will be discussed in Section 4.3. Although the maximum contact force is not determined for this case as the simulated radial crack keeps extending, the field test curve can be used as a reference for other simulated cases. Considering the discreteness of ice, the difference is within an acceptable range.

The trend of maximum ice load rising with impact speed is consistent with the test results, as shown in Figure 9. In the field test, this trend is obvious for β=50° , while the measured ice load of β=30° is quite discrete. The angle β between the landing craft bow and ice plate has a great influence on the ice load. As the angle β is larger, the bending load is smaller. Because as the vertical force component increases, it takes less total force to bend the ice plate. This trend proves the fact that a more inclined structure is more beneficial for the ice breaking. In addition, the contact force for crack initiation also shows a certain law. As the angle β decreases and velocity v increases, the force for crack initiation also increases, indicating similar trend with the crack propagation load. In addition, some simulated ice loads are lower than the field test data. According to Valanto [42-43], the maximum ice load is not reached instantaneously by the time ice breaks. Due to the intertia of the broken ice and surrounding water, the ice load continues to rise during the broken ice accelerating at higher interacting speed. Therefore, the simulated ice load until ice breaks could be lower than the measured load, where elastic foundation is used to simulate water, and the interacting speed is relatively high. And at lower interacting speed, it shows in Lu et al. [44] that using the elastic foundation will overestimate the ice breaking load. These clues indicate that further researches on hydrodynamics and broken ice movement are necessary.

Another evaluation criterion is the fracture size d, as shown in Figure 5. Figure 10 displays the tested and simulated maximum distance d from the bending fracture to the contact edge. The simulated fracture size d becomes smaller as the impact speed and angle β increase. In field tests, for the case of angle of β=30° and β=50° shown in Figure 10, the measured fracture size was around 1.5m to 2.0m, and doesn't show a clear trend for different impact velocity. Despite this, the simulated size of the fracture is very close to the test result.

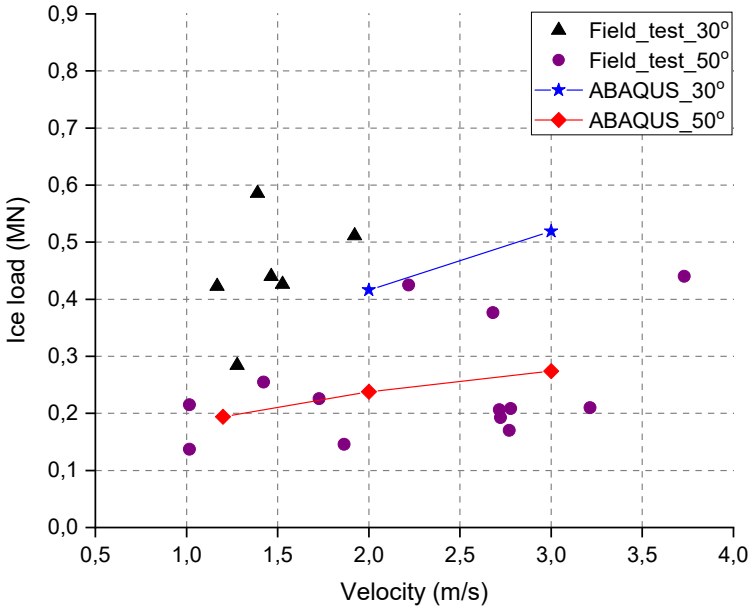

Figure 9. Comparison of the ice load of field test [14] and numerical simulations at different velocity v and different angle β.

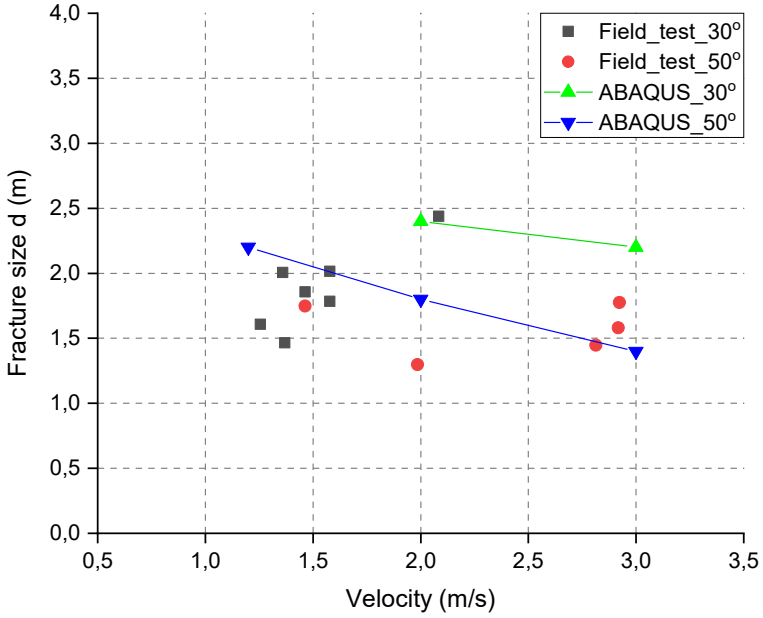

Figure 10. Bending fracture size d varying with velocity v under different angle β in field test [14] and numerical simulations.

4.2 Stress state and crack initiation of circumferential crack

The circumferential crack initiation and propagation processes are similar in all the cases. Take the case of β=50°, v=2m/s as an example, to illustrate the stress state of the ice plate before crack emerges and the crack initiation, as well as whether Tsai-Wu criterion can reflect the characteristics of the ice plate bending.

Figure 11 shows the distribution of Tsai-Wu failure function f on the top surface of the ice plate and its variation with time. When the value of f exceeds 1, crack will emerge at the corresponding location. The area prone to crack is located around the centerline, distributing along an annular band. After the

landing draft bow collides with the ice plate, the potential crack area continues to shift further along x axis, and the failure function f keeps increasing until the crack appears at some place in the midline.

While for the surface at the bottom of the ice plate, the area where the crack may initiate is located near the contact edge, which will be shown in Figure 14. Once it emerges, it will extends in radial direction. For the case of β=50°, v=2m/s until the crack initiation at the surface of the ice plate (t=7ms), the maximum value of f at the bottom is only 0.4. And during the top crack propagation, f at the bottom also doesn't reach 1. Therefore, the crack doesn't emerge at the bottom for this case. This simulated result is consistent with the phenomenon in the test, that bending failure is the dominant failure mechanism of ice plate.

In order to investigate the fracture mechanism of ice plate and further discuss whether the failure mechanism is well captured, it is necessary to discuss the stress state of ice before fracture. The stress in x direction S11 along the midline on top surface of the ice plate is shown in Figure 12. Under the combination of horizontal force compressing the ice plate in plane and vertical external forces bending the ice plate outside the plane, S11 near the contact area is compressive stress, then increases as the distance from contact edge increases. A tensile stress region is formed in the range of 0.3m to 4m from the edge. Then S11 decreases to be negative and rebounds to 0 eventually. The S11 curve can be compared with the analyzed results of Varsta [14] that is shown in Figure 13. In the analysis of [14], membrane elements are used. Although the material parameters and ice plate modeling are different, the stress distribution of both analyses present the same trend, and the values are quite close.

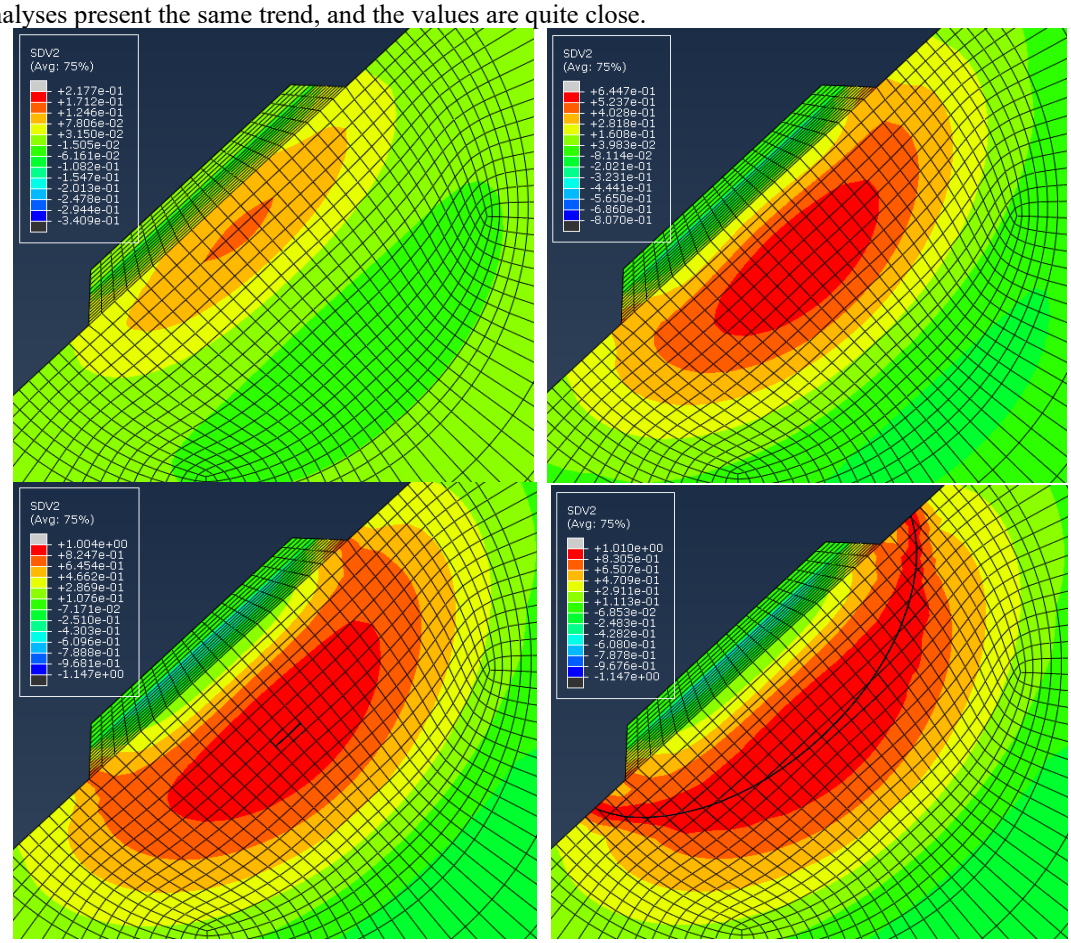

Figure 11. Distribution of crack initiation function f at the top surface of the ice plate. Time t=2ms, 5ms, 7ms, 12.2ms from contacting with the landing craft bow in the case of β=50°, v=2m/s.

In the previous investigations [45-46], it has been found that the tensile strength of ice is much smaller than its compressive strength, so the ice plate is prone to bending fracture induced by tensile failure. When the landing craft bow collides with ice plate in a certain angle, the ice plate is subjected to a vertical downwards force, causing that some part of the top surface of ice plate to be stretched. Once the tensile limit is exceeded, bending failure induced by stretching occurs. While for the ice plate simulated in this paper, it is symmetrical about x-axis, then S11 of the peak in Figure 12 is almost the maximum tensile stress in horizontal plane on the midline of the top surface. In the numerical simulation, the initial crack predicted by Tsai-Wu criterion emerges at the midline of the top surface, located at 1.8m from the contact

edge. This position is quite close to the position of the maximum S11 when the crack appears (7ms) in Figure 12. Thus for the simulation of ice plate bending, simulating initial crack using Tsai-Wu criterion corresponds well to the above maximum tensile stress mechanism of level ice. However, judging bending failure according to Tsai-Wu criterion is not equivalent to the maximum tensile stress criterion. Because Tsai-Wu criterion is based on three-dimensional stress space, taking six stress components of the element.

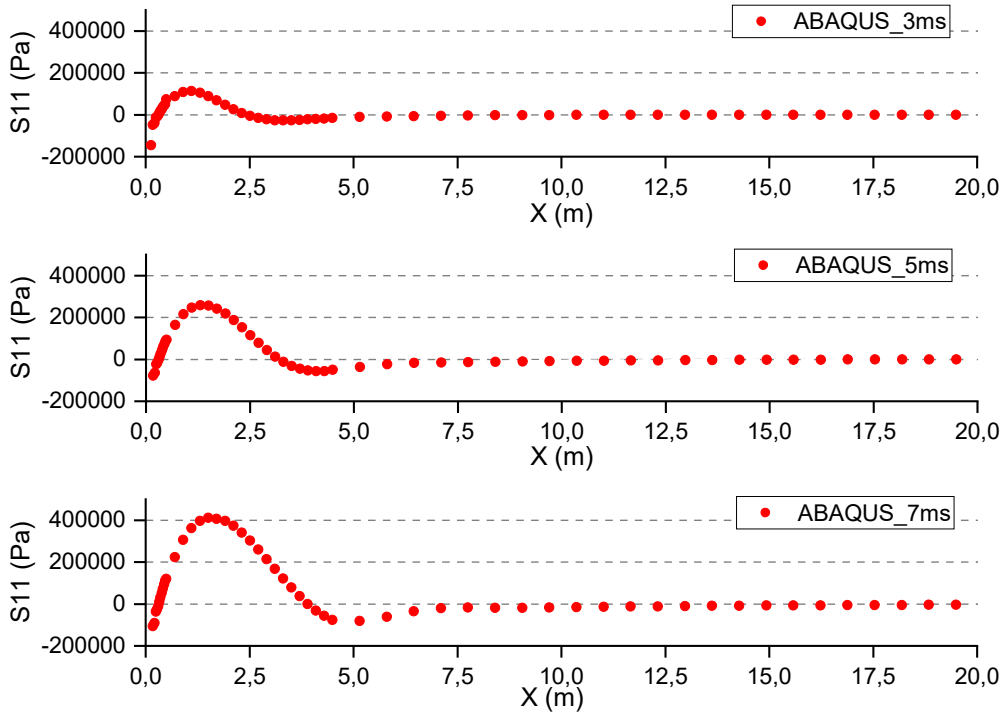

Figure 12. Stress in x direction S11 along the midline of top surface of ice plate calculated in ABAQUS for the case of β=50°, v=2m/s. The time 5ms and 7ms are the time after steel plate gets contact with the edge of ice plate. Positive value represents tension.

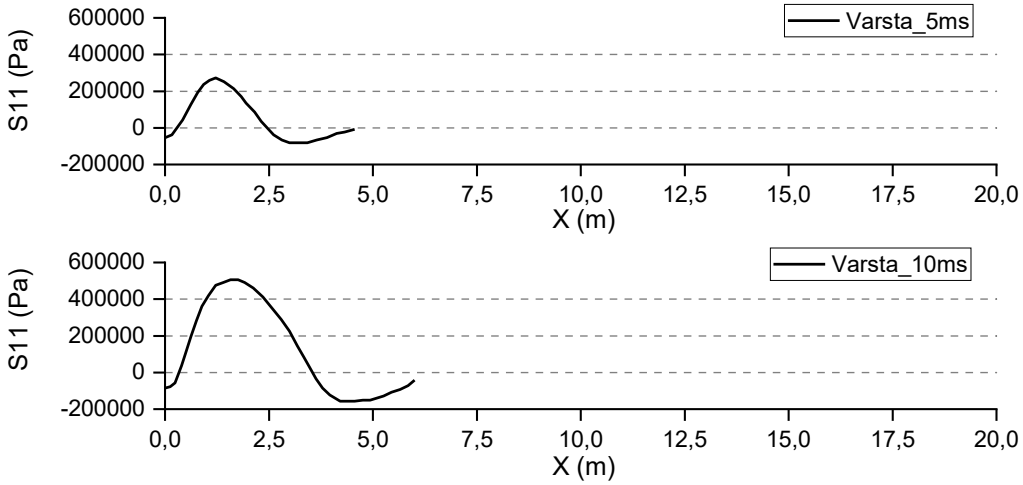

Figure 13. Stress in x direction S11 along the midline of top surface of ice plate obtained in [14] for the case of β=50°, v=2m/s.. 5ms and 10ms are the time after steel plate gets contact with the edge of ice plate. Positive value represents tension.

4.3 Competition between circumferential crack and radial crack

4.3.1 Competition mechanism

In the numerical simulations, circumferential crack and radial crack both emerge in certain cases. This chapter will discuss their formation mechanism, on which conditions different crack will emerge, such as collision speed and angle, as well as the features of their initiation and propagation.

At the top surface, the circumferential crack always emerges in the midline, then propagates towards free boundaries. While in the field test, it is not recorded that whether the bending crack emerges in the midline first, then propagates towards the free edges, or emerges near the free edge, or emerges at multiple places, due to the technical limitations at that time. Once the landing craft bow collides with the ice plate,

bending failure occurs in a very short time. But it is claimed in [14] that the circumferential crack is the dominant failure mode, and breaking the ice plate into two pieces from the bottom (splitting) is not observed during the test with varied speed.

In the numerical simulation, the ice plate is pressed downwards under the external load, and the bottom surface close to the contact edge of the ice plate is also in a tensile state. This makes it possible to breakage here. It is found that there is a competition between the radial crack and circumferential crack in the numerical simulation, which means both cracks may occur and interact with each other. For most of the cases simulated in this paper, the crack initiation criterion f of the area at the bottom edge is far from 1 at the time of a crack initiates at the top. And after the circumferential crack starts to propagate, the tensile state of the bottom ice is relieved, so the radial crack doesn't emerge.

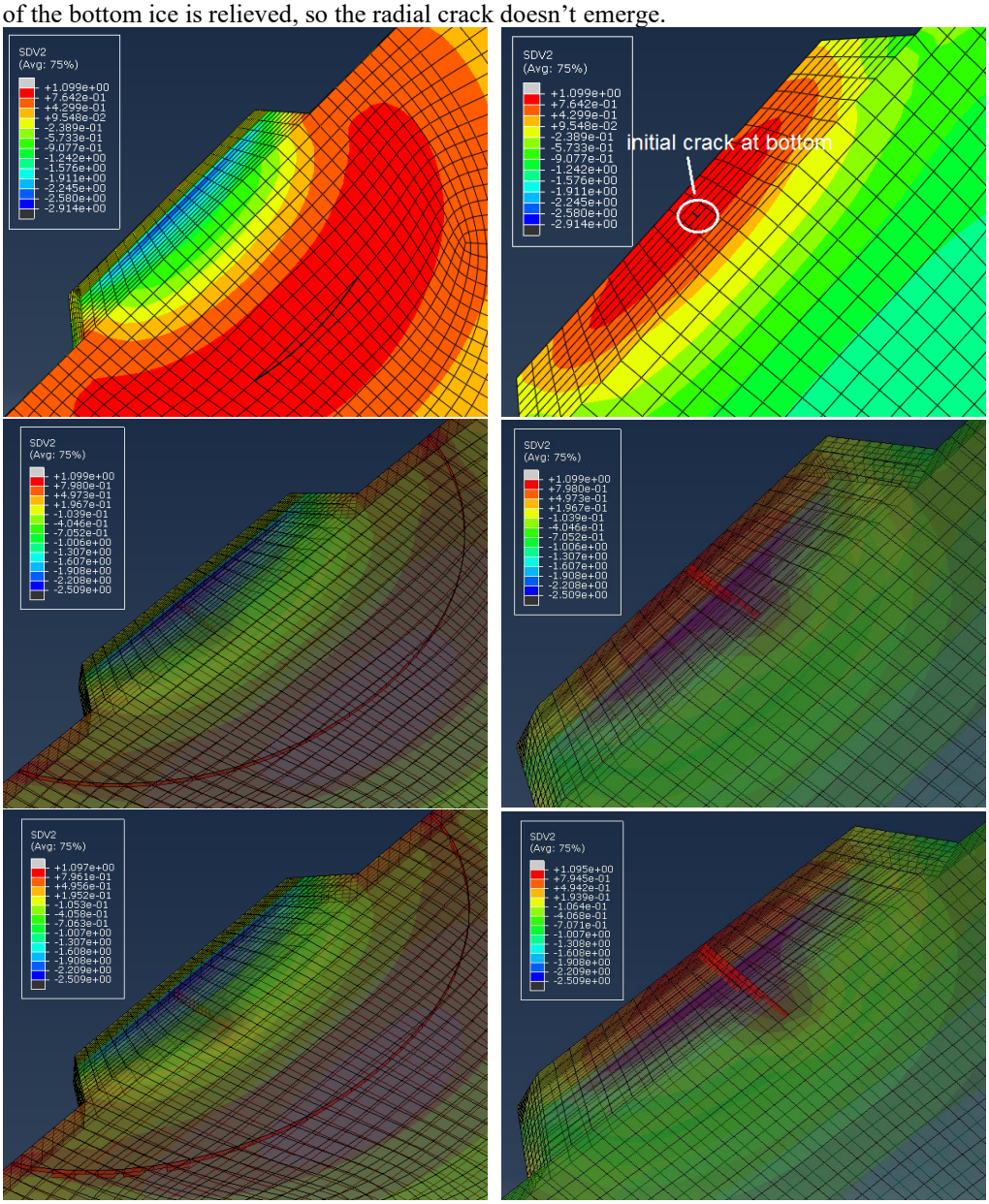

Figure 14. Tsai-Wu crack initiation criterion f at the top surface (left) and the bottom surface (right) of the case β=30°, v=2m/s. First row represents the crack initiation at 10ms, second and third rows represents the crack propagation at 14ms and 16ms respectively.

While in the cases of β=30°, v=2m/s, simulated initial cracks emerge both at the top surface and at the bottom edge. In Figure 14, it is shown that the values of f of the bottom edge near the contact area and of the top surface get close to 1 almost at the same time. It can be seen that the crack at bottom is vertical to the contact edge, and has a tendency to expand along the radial direction. Both circumferential crack and radial crack are vertical to direction of the maximum tensile stress. Along with the circumferential crack propagates, the crack at the bottom is also propagating, both in the horizontal direction and along the ice thickness direction. In the second row of Figure 14, when the circumferential crack propagates through

the top surface, the radial crack penetrates two layers of ice elements in thickness direction near the edge. And in the third row of Figure 14, the radial crack propagates further in horizontal direction and penetrates three layers of elements in thickness direction, and circumferential crack also begins to penetrate downwards. The case of β=30° , v=1.2m/s is also simulated in our research. In this case, the circumferential crack does not form, and the radial crack emerges first.

The difference between the numerical simulation and the field test of this two cases may come from several factors. First, the hydrodynamic force of water is not considered in the simulation. The dynamic "bedding" under the level ice influences the time-dependent deformation of level ice, affecting the distribution of stress and strain, thus the location and timing of the initial crack, the crack propagating process as well as the ice load. With sufficient consideration of water, cracks may not appear at the bottom of level ice, and the crack development could also be influenced. Second, there is a temperature difference between the upper and lower surfaces of the level ice, so the mechanical properties in vertical direction is gradient. Then gradient material parameters and failure criterion may be necessary to verify how this property affects the level ice behavior. Another possibility is that in the field test, along with the circumferential crack forms, radial cracks at the bottom may also emerge, but their expansion is suppressed, so the ice does not break in this way and only some damage exists at the bottom. In the ship-ice plate interaction process, as shown in literatures [47-48], the two forms of fracture are usually symbiotic, but it is not certain whether initial crack at the bottom has occurred during bending. After the occurrence of bending failure, the boundary condition of the peeled off ice plate changes, then a second failure (splitting) occur due to the contact with the ship hull and surrounding ice, as well as the influence of water. In any case, for the ice plate simulated in this paper, breaking into two pieces is not the mechanism dominating the maximum ice load. Because the rectangular ice plate is fixed in three boundaries and pressed downwards by the landing craft bow, the radial crack can not keep expanding and reach the fixed boundaries, then becomes the final failure mechanism that determine the maximum ice load. Even if the radial crack appears first and keeps crack propagating, bending crack should emerge at a certain timing and terminate the ice load rising. Due to the difficulty of numerical simulation, it is not proved in this paper whether and when the circumferential crack occurs in the case of the bottom crack emerges first.

4.3.2 Influence of impact angle β and velocity v

Table 4 summarizes the maximum f along the midline of the upper surface and along the midline of the lower surface respectively. It could be clearly seen that for β=50° , the top f is significantly higher than the bottom f, so a circumferential crack always emerges. And as the impact speed increases, the top f is much higher than bottom f. There is a similar trend for the cases of β=30° . While f for β=30° at the two locations are relatively close, and top f is higher when the speed is high.

The impact speed and angle will not only affect the ice load, but also the competition of the ice fractures. For all the cases of β=50° , crack at the bottom never emerges. For cases of β=30° , only radial crack emerges at v=1.2m/s , and only circumferential crack emerges at v=3m/s , while both cracks emerge at v=2m/s . It can be concluded that as the velocity is higher, or the landing craft bow is titled more horizontally, the ice plate is more inclined to bending, otherwise a crack may initiate at the bottom.

Table 4. Maximum crack initiation function f along the midline of the upper surface and lower surface.

case	top f		bottom f	
	value	location x (m)	value	location x (m)
β=30°, v=1.2m/s	0.814	2.91	1.001	0.15
β=30°, v=2m/s	1.029	2.31	0.989	0.15
β=30°, v=3m/s	1.005	2.11	0.945	0.15
β=50°, v=1.2m/s	1.005	2.11	0.744	0
β=50°, v=2m/s	1.004	1.71	0.439	0
β=50°, v=3m/s	1.005	1.307	0.262	0

5. Conclusion

This paper uses extended finite element method (XFEM) in ABAQUS to simulate a field test where an inclined landing craft bow impact on level ice in Baltic Sea. Transversely isotropic elastic material model is adopted for the constitutive relation of ice bulk elements, and transversely isotropic Tsai-Wu criterion is for the prediction of the initiation of the crack. Once the crack initiates, cohesive surface concept with traction-separation curve is used for the description of crack propagation. The contact force is simplified as a monotonously increasing force. And dynamic implicit analysis is used for the simulation.

Numerical simulation of the impact is carried at different speeds (1.2m/s, 2m/s, 3m/s) and different collision angles (30^{o} , 50^{o}). The stress state of the level ice before cracking, the location of the initial crack, and crack propagation path and ice load can be obtained. Main conclusions are as follow:

1. In the impact with landing craft bow, the level ice deformation can be divided into three phases: continuous deformation, crack initiation, crack propagation. Before cracking, the crack potential area represented by Tsai-Wu criterion shifts away from the contact region, and *f* value is increasing, until initial crack emerges at the midline of the top surface of ice plate. Then the crack propagates towards free boundary in the direction perpendicular to the maximum principle stress, and finally an arcuate crack forms. The simulated bending crack is consistent with the field test.
2. The impact velocity and inclination of the landing craft bow have a great influence on the cracking process in the numerical simulation. Contact force of the circumferential crack penetrating through the upper surface of ice plate is taken as the bending load. At the same inclination, as the collision velocity increases, the bending load increases, and the time from contact to bending as well as the distance of the initial crack from the contact edge decrease. While for the same velocity, as the angle β between the landing craft bow and level ice increases, the ice load decreases, indicating that the ice plate is more easily bent, and the fracture size is reduced. In addition, the time required for bending in numerical simulation is also in good agreement with the field test.
3. In numerical simulations, the competition between the circumferential crack and the radial crack is found. For the case of β=30^{o}, v=2m/s , crack appears simultaneously from the top and bottom of the ice plate. Top crack propagates as a circumferential crack. The bottom initial crack is located closely to the contact area and perpendicular to the contact edge, having a trend to propagate in the radial direction. The competition is related with the impact speed and inclination of the landing craft bow. If the speed is higher and the angle β is larger, only circumferential crack emerges. While if the speed is lower and the angle β is smaller, such as the case above, radial crack may initiate at the bottom of the level ice.

Acknowledgement

This work was financially supported by the National Key Research and Development Program of China (Grant number 2016YFC0303405) and China Scholarship Council. The authors are sincerely grateful to the support.

6. Reference

1. Lindquist A. Straightforward method for calculation of ice resistance of ships. POAC'89. 1989.
2. Kerr AD. The bearing capacity of floating ice plates subjected to static or quasi-static loads. Journal of glaciology. 1976;17(76):229-268.
3. Kerr AD. The critical velocities of a load moving on a floating ice plate that is subjected to in-plane forces. Cold Regions Science and Technology. 1983 Feb 1;6(3):267-274.
4. Kerr AD, Palmer WT. The deformations and stresses in floating ice plates. Acta Mechanica. 1972 Mar 1;15(1-2):57-72.
5. Kerr AD. On the determination of horizontal forces a floating ice plate exerts on a structure. Journal of Glaciology. 1978;20(82):123-134.
6. Su B, Riska K, Moan T. A numerical method for the prediction of ship performance in level ice. Cold Regions Science and Technology. 2010 Mar 1;60(3):177-88.
7. Su B, Riska K, Moan T. Numerical simulation of local ice loads in uniform and randomly varying ice conditions. Cold Regions Science and Technology. 2011 Feb 1;65(2):145-59.
8. Zhou L, Gao J, Li D. An engineering method for simulating dynamic interaction of moored ship with first-year ice ridge. Ocean Engineering. 2019 Jan 1;171:417-28.
9. Lubbad R, Løset S. A numerical model for real-time simulation of ship–ice interaction. Cold Regions Science and Technology. 2011 Feb 1;65(2):111-27.
10. Erceg S, Ehlers S, und Polach RV, Leira B. A numerical model to initiate the icebreaking pattern in level ice. ASME 2014 33rd International Conference on Ocean, Offshore and Arctic Engineering 2014 Jun 8 (pp. V010T07A017-V010T07A017). American Society of Mechanical Engineers.
11. Wang Y, Poh LH. Velocity effect on the bending failure of ice sheets against wide sloping structures. Journal of Offshore Mechanics and Arctic Engineering. 2017 Dec 1;139(6):061501.
12. Ehlers S, Kujala P. Optimization-based material parameter identification for the numerical simulation of sea ice in four-point bending. Proceedings of the Institution of Mechanical Engineers, Part M: Journal of Engineering for the Maritime Environment. 2014 Feb;228(1):70-80.
13. Sazidy MS. Development of velocity dependent ice flexural failure model and application to safe speed methodology for polar ships (Doctoral dissertation, Memorial University of Newfoundland). 2015
14. Varsta P. On the mechanics of ice load on ships in level ice in Baltic Sea. 1983.

15. Lu W, Heyn HM, Lubbad R, Løset S. A large scale simulation of floe-ice fractures and validation against full-scale scenario. International Journal of Naval Architecture and Ocean Engineering. 2018 May 1;10(3):393-402.
16. Lu W, Lubbad R, Løset S, Høyland KV. Cohesive zone method based simulations of ice wedge bending: a comparative study of element erosion, CEM, DEM and XFEM. InThe 21st IAHR International Symposium on Ice 2012 (pp. 920-938).
17. Abaqus V. 6.14, Online Documentation Help, Theory manual: Dassault Systms. Accessed on. 2016 May.
18. Pommier S, Gravouil A, Moes N, Combescure A. Extended finite element method for crack propagation. John Wiley & Sons; 2013 Mar 4.
19. Lu W, Lubbad R, Løset S. Simulating ice-sloping structure interactions with the cohesive element method. Journal of Offshore Mechanics and Arctic Engineering. 2014 Aug 1;136(3):031501.
20. Kuutti J, Kolari K, Marjavaara P. Simulation of ice crushing experiments with cohesive surface methodology. Cold Regions Science and Technology. 2013 Aug 1;92:17-28.
21. Konuk I, G rtner A, Yu S. A Cohesive Element Framework for Dynamic Ice-Structure Interaction Problems—Part I: Review and Formulation. InASME 2009 28th International Conference on Ocean, Offshore and Arctic Engineering 2009 Jan 1 (pp. 33-41). American Society of Mechanical Engineers.
22. Konuk I, G rtner A, Yu S. A Cohesive Element Framework for Dynamic Ice-Structure Interaction Problems—Part II: Implementation. InASME 2009 28th International Conference on Ocean, Offshore and Arctic Engineering 2009 Jan 1 (pp. 185-193). American Society of Mechanical Engineers.
23. Wang F, Zou ZJ, Zhou L, Ren YZ, Wang SQ. A simulation study on the interaction between sloping marine structure and level ice based on cohesive element model. Cold Regions Science and Technology. 2018 May 1;149:1-5.
24. Mulmule SV, Dempsey JP. Stress-separation curves for saline ice using fictitious crack model. Journal of engineering mechanics. 1997 Aug;123(8):870-7.
25. Mulmule SV, Dempsey JP. A viscoelastic fictitious crack model for the fracture of sea ice. Mechanics of Time-Dependent Materials. 1997 Dec 1;1(4):331-56.
26. Mulmule SV, Dempsey JP. Scale effects on sea ice fracture. Mechanics of Cohesive-frictional Materials: An International Journal on Experiments, Modelling and Computation of Materials and Structures. 1999 Nov;4(6):505-24.
27. Dempsey JP, Tan L, Wang S. An isolated cohesive crack in tension. Continuum Mechanics and Thermodynamics. 2010 Sep 1;22(6-8):617-34.
28. Dempsey JP, Cole DM, Wang S. Tensile fracture of a single crack in first-year sea ice. Philosophical Transactions of the Royal Society A: Mathematical, Physical and Engineering Sciences. 2018 Aug 20;376(2129):20170346.
29. Xu Y, Hu Z, Ringsberg JW, Chen G, Meng X. An ice material model for assessment of strain rate, temperature and confining pressure effects using finite element method. Ships and Offshore Structures. 2018 Dec 5:1-1.
30. Derradji-Aouat A. Multi-surface failure criterion for saline ice in the brittle regime. Cold regions science and technology. 2003 Mar 1;36(1-3):47-70.
31. Zhou Z, Ma W, Zhang S, Mu Y, Zhao S, Li G. Yield surface evolution for columnar ice. Results in Physics. 2016 Jan 1;6:851-9.
32. Liu Z, Amdahl J, Løset S. Plasticity based material modelling of ice and its application to ship–iceberg impacts. Cold regions science and technology. 2011 Mar 1;65(3):326-34.
33. Gao Y, Hu Z, Ringsberg JW, Wang J. An elastic–plastic ice material model for ship-iceberg collision simulations. Ocean Engineering. 2015 Jul 1;102:27-39.
34. Xu Y, Hu Z, Ringsberg JW, Chen G. Nonlinear viscoelastic-plastic material modelling for the behaviour of ice in ice-structure interactions. Ocean Engineering. 2019 Feb 1;173:284-97.
35. Browne T, Taylor R, Jordaan I, Gürtner A. Small-scale ice indentation tests with variable structural compliance. Cold Regions Science and Technology. 2013 Apr 1;88:2-9.
36. Gagnon RE. Analysis of visual data from medium scale indentation experiments at Hobson's Choice Ice Island. Cold Regions Science and Technology. 1998 Aug 1;28(1):45-58.
37. O'Rourke BJ, Jordaan IJ, Taylor RS, Gürtner A. Experimental investigation of oscillation of loads in ice high-pressure zones, part 1: single indentor system. Cold Regions Science and Technology. 2016 Apr 1;124:25-39.
38. Liu H W, Miller K J. Fracture Toughness of Fresh-Water Ice. Journal of Glaciology, 1979, 22(86):135-143.
39. Vincent M R, Dempsey J P. Fracture energy of saline ice. Ice in Surface Waters, 1998: 567-573.
40. Zhang M, Zhang D, Goerlandt F, Yan X, Kujala P. Use of HFACS and fault tree model for collision risk factors analysis of icebreaker assistance in ice-covered waters. Safety science. 2019 Jan 1;111:128-43.

41. Zhang M, Zhang D, Fu S, Yan X, Goncharov V. Safety distance modeling for ship escort operations in Arctic ice-covered waters. Ocean Engineering. 2017 Dec 1;146:202-16.
42. Valanto, P. Experimental study of the icebreaking cycle in 2-D. Proceedings of the 8th International Offshore Mechanics and Arctic Engineering Symposium, The Hague, Netherlands. 1989: 343–349.
43. Valanto, P. On the cause and distribution of resistance forces on ship hulls moving in level ice. Proceedings of POAC. 2001: 803–816.
44. Lu W, Løset S, Lubbad R. Ventilation and backfill effect during ice–sloping structure interactions. Proceedings of the 21st International Symposium on Ice (IAHR), Dalian, China. 2012: 826-841.
45. Petrovic JJ. Review mechanical properties of ice and snow. Journal of materials science. 2003 Jan 1;38(1):1-6.
46. Timco GW, Weeks WF. A review of the engineering properties of sea ice. Cold regions science and technology. 2010 Feb 1;60(2):107-29.
47. Li F, Kotilainen M, Goerlandt F, Kujala P. An extended ice failure model to improve the fidelity of icebreaking pattern in numerical simulation of ship performance in level ice. Ocean Engineering. 2019 Mar 15;176:169-83.
48. Li F, Goerlandt F, Kujala P, Lehtiranta J, Lensu M. Evaluation of selected state-of-the-art methods for ship transit simulation in various ice conditions based on full-scale measurement. Cold Regions Science and Technology. 2018 Jul 1;151:94-108.